IEEE Access
Multidisciplinary | Rapid Review | Open Access Journal

Received March 11, 2020, accepted March 30, 2020, date of publication April 6, 2020, date of current version April 22, 2020.

Digital Object Identifier 10.1109/ACCESS.2020.2985705

Monitoring Neural Activities in the VTA in Response to Nicotine Intake Using a Novel Implantable Microimaging Device

YOSHINORI SUNAGA[1], YASUMI OHTA[2], YASEMIN M. AKAY[1], (Member, IEEE), JUN OHTA[2], (Senior Member, IEEE), AND METIN AKAY[1], (Fellow, IEEE)

[1]Department of Biomedical Engineering, University of Houston, Houston, TX 77204, USA
[2]Division of Materials Science, Graduate School of Science and Technology, Nara Institute of Science and Technology, Ikoma 630-0192, Japan

Corresponding author: Metin Akay (makay@uh.edu)

This work was supported in part by the University of Houston, and in part by the Japan Society for the Promotion of Science (JSPS) under Grant 17H06866.

ABSTRACT Measurements of the deep brain area of rodents has been one of the most important methods to study deep brain activities, in part due to limited access of this region. In order to address this problem, we have designed and fabricated an implantable microimaging device for fluorescence imaging in the deep brain of rodents. In this study, we established a new fabrication method of a flat and uniformed fluorescence filter for an implantable microimaging device which obtained higher quality images, and aimed to show the performance of the device in the ventral tegmental area (VTA) of rats. We introduced GCaMP6s in the VTA of rats by adeno-associated viral (AAV) injection. The change in the fluorescence intensity was associated with nicotine administration and was observed by using our custom implantable microimaging device. We showed that nicotine administration significantly affected the excitation of DA neurons in different sub-regions of the VTA, reaching a maximum activation between 6-10 minutes following nicotine exposure, followed by a decrease after 31-35 minutes. Therefore, we believe our implantable microimaging device can potentially be used to monitor the neural activation within the sub-regions of the VTA in response to acute nicotine exposure by using GCaMP.

INDEX TERMS Nicotine, dopamine, VTA, implantable imaging device, fluorescence imaging, GCaMP.

I. INTRODUCTION

Nicotine intake due to smoking is well-known to negatively affect the health of the human brain and body; the interaction of nicotine with dopamine (DA) neurons is well established in the field of neuroscience. Previous studies have determined that perinatal nicotine exposure affects DA release and subsequent DA levels and turnover in the fetal forebrain [1]–[3]. After nicotine injection, some ventral tegmental area (VTA) DA neurons showed different temporal firing rates. Altogether, these results suggest that detailed subgroups of VTA DA may exist within VTA, defined by physical function and/or anatomical sub-region, including parabrachial pigmented nucleus (PBP), parainterfascicular nucleus (PIF) and paranigral nucleus (PN) [4]–[7]. Our previous electrophysiology study showed higher neural activity in the PIF sub-region in response to nicotine exposure [8]. However, several other studies suggested that the posterior VTA, and not the anterior VTA centering on the PN, mediates the rewarding effects of drugs including nicotine [7]. Therefore, to clarify the controversial findings on which region plays the most critical role in the reward pathway, we aimed to visualize the areas of the VTA, particularly the neural activities of PIF and PN. We believe that this information is critical to determine the neuronal circuits and the interaction of neurons in the VTA In the last few decades, optical imaging methods have accelerated the discovery of neuronal mechanisms [9]–[12]. In particular, fluorescence imaging technology has proven to be an especially powerful tool to observe brain function. However, optical imaging tools are generally larger in device size, and are more invasive than electrophysiological methods. Therefore, it has been difficult to gain access to the deep brain region (e.g. VTA). Even though these methods are limiting, several studies have developed deep brain imaging techniques, including microimaging devices based on optical fiber systems. These optical fiber systems have been found

The associate editor coordinating the review of this manuscript and approving it for publication was Henry Hess.

to be useful for monitoring brain functions given these high-quality images can be obtained with a conventional optical microscope.

One main advantage of both optical fiber and fluorescence microscopy platforms is to obtain high-quality deep brain imaging.

However, an optical fiber platform is rather rigid compared to an electrical wire, and therefore may hinder the use of it to record neural activities from freely moving animals [13]–[16]. On the other hand, an ultra-small fluorescence microscope mounted on a rodent head [11], [17] provides a relatively large view with spatial resolution on the micrometer scale when a glass rod lens or GRIN lens is inserted. In addition, electrical cables do not hinder the rodent's movement in this category of devices. However, the system weighs ∼2 g, which is approximately 10% of the weight of a typical mouse, making it unsuitable for behavioral studies [11], [17]. Furthermore, these methods only allow us to observe the horizontal plane, making data collection within the vertical plane challenging.

Recently, Lu *et al.* developed a wireless, injectable fluorescence photometry system for deep-brain fluorescence recordings in untethered and freely behaving animals. The proposed system integrates a miniaturized light source ($270 \times 220 \times 50$ μm) and a photo detector ($100 \times 100 \times 5$ μm) placed adjacent to one another on a thin, narrow, and flexible polyimide substrate. The results suggested that the platform can be used in in vivo studies with untethered and freely moving animals to record calcium fluorescence in the deep brain, though it only provides imaging data from one photodiode on a region of interest. However, its performance was comparable to or better than those of fiber photometry systems [18].

To monitor the neural activation within the sub-regions of the VTA, we recently proposed and developed a novel microimaging device, consisting of an ultra-small CMOS image sensor and micro-LEDs on a flexible printed circuit (FPC) substrate made of polyimide that can be directly implanted into the brain [19]. The entire device surface is coated with Parylene-C for biocompatibility and to make it waterproof. This sensor is lightweight (∼0.05 g), and therefore permits the rat to move freely and be able to swim. Because it is thin and lightweight, the device can be implanted in the deep brain region of the rat, such as the VTA (Fig. 1). At least two devices can be used simultaneously to investigate the mechanism of the neural network in the brain. It contains no optics for imaging and can detect only those fluorescence objects that are near the device surface. To obtain high quality fluorescence images, an effective fluorescence filter with a high excitation light rejection performance was required. Especially, the thickness and shape of the filter directly influences imaging quality. To miniaturize the size of the device, it contains no optics for imaging and can detect only those fluorescence objects that are near the device surface. Subsequently, the mixed chemical solution of yellow dye and resin which acted as a fluorescence filter was coated on the surface of the imaging area. However, the image quality can be degraded due to the uneven filter shape.

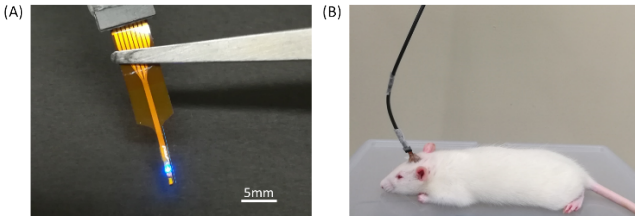

FIGURE 1. Implantable microimaging device for minimally invasive deep brain in vivo imaging. (A) Photograph of the microimaging device with illuminated LEDs (473nm). Scale bar is 5 mm. (B) Representative picture of a rat after the device implantation into the VTA. A wire cable is connected to the device from a control board.

Therefore, in this study, we improved our implantable microimaging device by preparing a custom-made fluorescence filter to suppress the excitation light. This new minimally invasive device improved the fluorescent image quality and enabled us to examine neural activation of DA neurons in the VTA in response to nicotine exposure. Furthermore, this microimaging device allows us to observe the fluorescence in the vertical plane direction, which is traditionally difficult using conventional measurement methods, such as a standard fluorescence microscope.

II. METHODS

A. ANIMAL TREATMENT

All experiments were performed in accordance with the protocols approved by the Institutional Animal Care and Use Committee (IACUC) and the University of Houston Animal Care Operations (ACO). Female Sprague–Dawley (SD) rats (Charles River) ($n = 5$) were maintained on a 12-h light/12-h dark schedule in 22±2°C and 65% humidity. Access to standard food and water was *ad libitum*. In all surgeries, animals were mounted in a stereotaxic apparatus (Narishige), and body temperature was maintained at 36-37°C with a homeothermic blanket system (Harvard Apparatus).

B. IMPROVEMENT OF THE IMPLANTABLE IMAGING DEVICE

The implantable microimaging device was designed for observation of a rodent's brain [19]–[24]. The microimaging device has an image sensor, LEDs as excitation light source (473 nm), and a fluorescence filter to reject excitation light. These parts were mounted on a flexible printed circuit (FPC, Taiyo Industrial Co.). Wires were protected by epoxy resin, and the whole device was further coated with Parylene-C to add biocompatibility and water protection (Fig. 2(A), (B)).

Compared to an ultra-small fluorescent microscopy that can be mounted on a rodent head [9]–[12], our smaller implantable device is also head-mountable. Additionally, our device weighs ∼0.05g, which is much lighter than those of currently available ultra-small fluorescent microscopy, which is about 2 g [11]. Overall, our device does not limit the rat's movements and reduces the overall invasiveness to the brain. While conducting imaging experiments, image data

was acquired by connecting the device and a control board by wires; the image sensor and LEDs were driven by only 6 wires. This setup did not impact animal behavior. The image sensor was controlled by using a custom program in Visual Studio (Microsoft) and a dedicated control board. Light intensity of the LED was controlled by a current generator. The control board converted analog signals from the image sensor to 14-bit digital signals. In this experiment, the frame rate was set to 10 frames per second (fps).

The image sensor held 40 × 90 pixels (Fig. 2(C)) and was designed and fabricated by using the standard CMOS process (0.35−μm, 2-poly-4 metal CMOS; Austria Microsystems). The pixel size was 7.5 × 7.5 μm square, and the pixel area was 0.3 × 0.675 mm. The theoretical spatial resolution of the device is approximately 7.5 micrometers, which is almost the same size as a soma, which is sufficient to observe the activities of cells. However, our previous in vitro experimental study indicated that the actual spatial resolution of the microimaging device is 22.3 ± 0.5 μm [20].

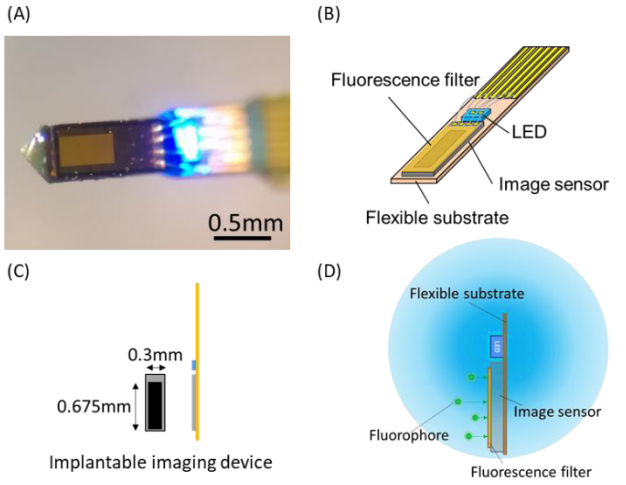

FIGURE 2. Details of an implantable microimaging device. (A) Photograph of the implantable microimaging device. Scale bar is 0.5 mm. (B) Schematic of cross-sectional view of the microimaging device. The image sensor surface was covered by the fluorescence filter. The LED was used to produce the excitation light source (473 nm). The device was coated with Parylene-C for biocompatibility and water protection. (C) Schematic of an implantable microimaging device with 0.675 mm height and 0.3 mm width. (D) Concept of the fluorescence imaging by an implantable microimaging device. Excitation light from LED was scattered by brain tissue and excited fluorophores in front of the microimaging area of the device.

The dimension of the image sensor chip was 0.45 × 1.53 × 0.125 mm, and its weight was less than 0.05 g. We used 305 × 280 μm LEDs (EPISTAR Corp.) with an emission wavelength of 473 nm as excitation light source. In this study, we used only one LED to reduce invasiveness to the brain and avoid penetration to the bottom of the brain. The excitation light from the LED was scattered by brain tissue, but was still used to excite fluorophores in front of the device imaging area (Fig. 2(D)). Our preliminary data determined that the rise of the LED's temperature was less than 1.2 °C, as measured by placing a thermocouple directly on the LED of the implantable device. We integrated the image sensor, LEDs and the fluorescence filter onto a specially designed flexible substrate.

In our previous studies, the fluorescence absorbing dye and the resin were dissolved in a solvent and the mixed solution was spin-coated directly on the image sensor, making image surface uneven and non-uniform [22]. Since the chip size was very small, the edge bead could easily occur, which could affect the image quality. The filter shape also became semi-cylindrical due to surface tension during the thermosetting process, causing degradation in the image quality.

Therefore, in this study, we designed and fabricated a flat and thinner fluorescence filter using new a fabrication method as shown in Figure 3. We first spin coated a cover glass (24 × 24 mm) with silicone resin (Norland Product Inc.) as a foundation (Fig. 3(A)). Then the yellow dye (Valifast yellow 3150 (Orient Chemical, Japan)), cyclopentanone (Wako, Japan), and the resin (NOA63, Norland Products, USA) were mixed at a weight ratio of 1:1:1. The mixed filter solution was applied to the spin coated silicone layer as a fluorescence filter (Fig. 3(B)). The coated film was soft-cured by heating to 100°C for 30 min. To make a flat filter, the middle area of the soft-cured filter, which was not influenced by edge bead, was cut to the appropriate size associated with microimaging device size by YAG laser (TNS Systems LLC, Figure 3(C)). The cut-filter was laid on microimaging device surface (Fig. 3(D)) and hard-cured by heating to 120°C for 120 min under air vacuum condition.

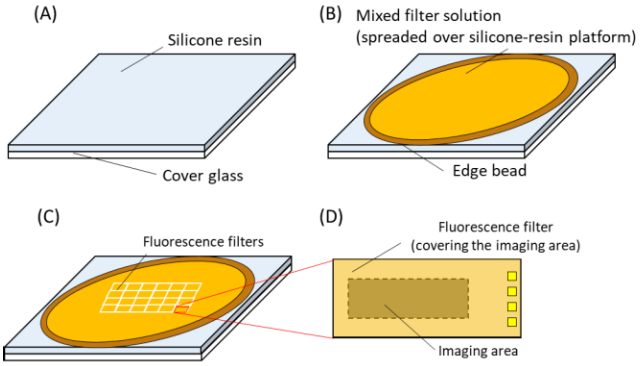

FIGURE 3. Fluorescence filter fabrication process. (A) shows the cover glass (24 × 24 mm) spin coated with the silicone resin. (B) The absorption (yellow) dye was mixed with cyclopentanone and the resin (NOA63). The mixture was applied to the spin coated silicone layer as a fluorescent filter. (C) shows the mixed solution (soft-cured filter), which was cut with the size of microimaging surface area. (D) shows the replacement of the hard-cured filter on top of the microimaging surface area.

C. AAV INJECTION SURGERY

In this study, to monitor calcium signals in DA neurons of the VTA, we used AAV-GCaMP6s (pAAV.CAG.GCaMP6s.WPRE.SV40, Addgene). AAV was introduced to the VTA by using a microinjection pump and a syringe with a microinjection needle (Fig. 4(A)). A burr hole was made at a position of VTA (anteroposterior (AP)= −5.2 mm, mediolateral (ML)= ± 0.8 mm, dorsoventral (DV) = −8.5 mm), and the virus was delivered to the site. After the virus injection, the needle

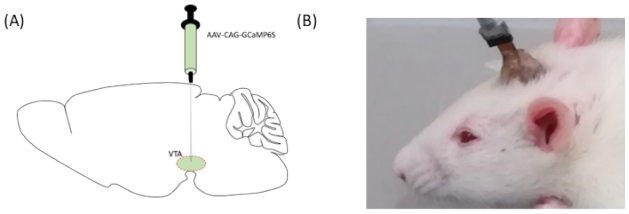

FIGURE 4. GCaMP6 injection and device implantation. (A) Schematic of the pAAV.CAG.GCaMP6s.WPRE.SV40 injection into both spheres. AAV was injected using a microinjector. (B) Representative photograph of a rat after the device implant surgery. Then the device was fixed onto the skull using dental cement.

was left in the injection position for at least 5 minutes to avoid diffusion delay. In this surgery, ketamine (90 mg/kg) and xylazine (10 mg/kg) were used at the recommended doses for anesthetics [25]. The rats were observed at least 2 weeks post procedure for the AAV infection.

D. DEVICE IMPLANTATION SURGERY

At least two weeks after AAV injection surgery, the microimaging device was implanted into the VTA. Ketamine (90 mg/kg) and xylazine (10 mg/kg) were used at the recommended doses [25]. The device was fixed to the rodent's skull using dental cement (Super Bond C&B, Sun Medical Co., LTD., Fig. 4(B)). The burr hole for the AAV injection surgery was slightly expanded using a microdrill to insert the microimaging device using a manipulator with minimal damage into the VTA position. The rat's scalp was sutured to cover the adhesive part and to avoid being peeled off during grooming.

E. GCaMP IMAGING EXPERIMENT

To monitor calcium signals in DA neurons of the VTA associated with nicotine administration, we introduced GCaMP6 into VTA two weeks before the custom-made implantable microimaging device was inserted. The implantation of the device in the VTA captured simultaneous delivery of the 473 nm excitation light and collected GCaMP fluorescence emission. This device also enabled the observation of the vertical plane of the brain, which has been historically difficult to achieve with conventional methods. We obtained data from the rat brains before and after nicotine (nicotine hydrogen tartrate salt, Sigma-Aldrich) solution administration (0.07 mg/kg, 0.21 mg/kg, and 0.63 mg/kg) for representative animals by intraperitoneal (IP) injection. Similar observation was made for the other animals in our study (n=5). We used the data collected prior to the nicotine administration as the control. Isoflurane (2.5%) was used as an anesthetic for 2-3 minutes before administering the nicotine dose to avoid animal discomfort and movement, and prevented the disconnection of the cables from the device. The data was obtained using a collection rate of 10 fps from unrestrained animals.

For the GCaMP fluorescence imaging measurements, changes in fluorescence intensity in the VTA were measured by using the pixel value of the implantable microimaging

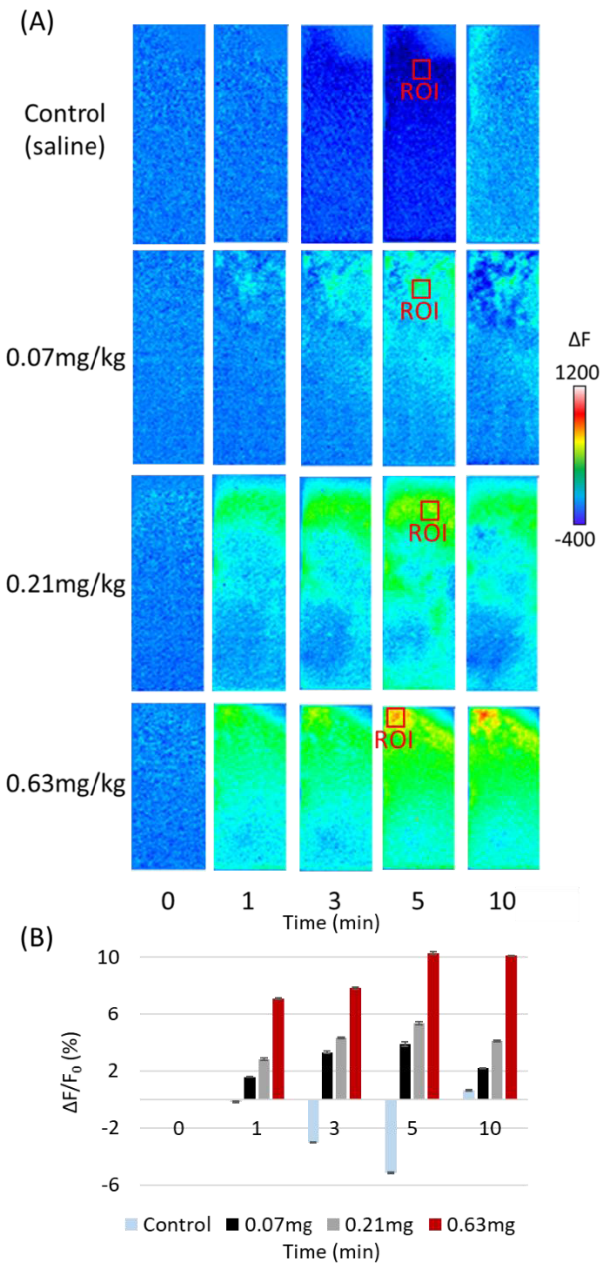

FIGURE 5. GCaMP fluorescence imaging associated with nicotine administration in the VTA. (A) Time-lapse fluorescence images of the rat's VTA administered with 0.07 mg/kg, 0.21 mg/kg, 0.63 mg/kg of nicotine and the control group (i.e. before nicotine administration). Nicotine was introduced by IP injection. (B) The graph of the fluorescence ratio of ROI, $\Delta F/F_0$ (%), (9 × 9 pixels) administered with 0.07 mg/kg, 0.21 mg/kg, and 0.63 mg/kg of nicotine and the control group. It should be noted that the fluorescence intensity increased with increased nicotine administration.

device. When the rat received nicotine, DA neurons in VTA were excited and GCaMP fluorescence increased. The fluorescence difference (ΔF) was defined as the difference between F and F_0. F_0 was the average fluorescence intensity within the region of interest (ROI, 9 × 9 pixels) in the reference image collected at time zero (t=0) (i.e. immediate before nicotine administration). F was the average value of the same

ROI after nicotine administration. The fluorescence ratio was calculated as $\Delta F/F_0$ (Eq.1). Fig. 5(A) and Fig. 6(A) indicated $\Delta F/F_0$ by using pseudo color. The values in Fig. 5(B) and Fig. 6(B) indicated the fluorescence ratio (%), $\Delta F/F_0$, of the ROI.

$$\frac{\Delta F}{F_0} = \frac{F - F_0}{F_0} \quad \text{(Eq. 1)}$$

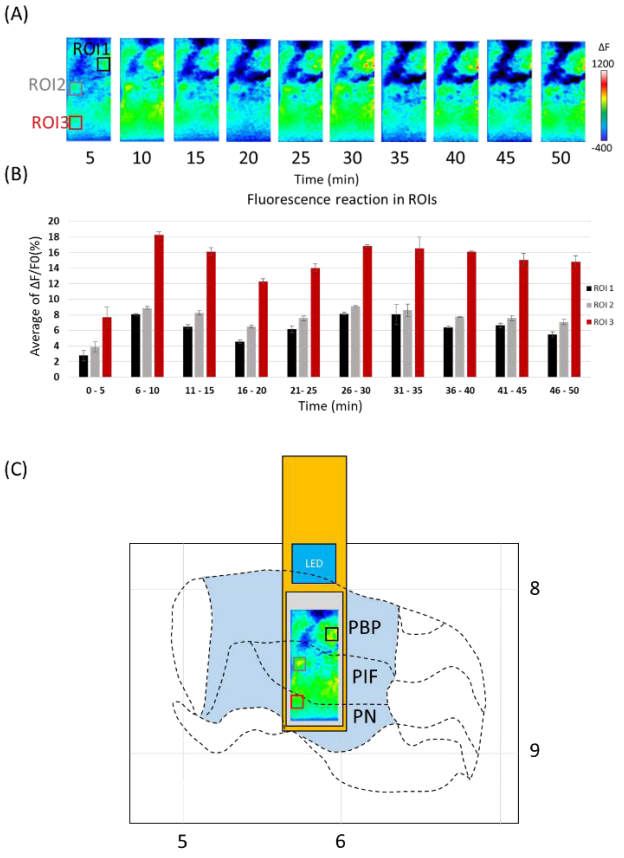

FIGURE 6. GCaMP fluorescence imaging activity from a representative rat associated with nicotine administration into the VTA. (A) Time-lapse fluorescence images of a rat after 0.63 mg/kg nicotine administration. Nicotine was introduced by IP injection. (B) A representative $\Delta F/F_0$ (%) graph shows the change in the fluorescence ratio after 0.63 mg/kg of nicotine administration at ROI1-3 in the VTA. A significant increase in the fluorescence intensity in the first 10 minutes and a significant decrease after 15 minutes until the end of the measurement for 50 minutes was observed ($p<0.0001$). The error bars were given as standard error of the mean. (C) Schematic of implant-position for the implantable microimaging device. Imaging area covered PIF and PN sub regions.

In order to confirm the position of the device and the GCaMP appearance, we prepared brain slices by using a VT1200 semiautomatic vibrating blade vibratome (Leica) and obtained the brain slices 100 μm thick. The slices were fixed overnight with 4% paraformaldehyde (PFA, Thermo Fisher Scientific) before imaging using a fluorescence microscope (Olympus).

F. STATISTICAL ANALYSIS

Repeated measures analysis of variance (ANOVA) were used to identify statistically significant differences in fluorescence ratios at each time point. A p-value less than 0.05 was considered significant. All experiments were done in triplicates. Data is represented as mean ± standard deviation.

III. RESULTS

A. GCaMP6s IMAGING RELATED WITH DA NEURON AND NICOTINE INTAKE

In previous studies, several groups investigated the DA neuron activity associated with nicotine administration in the VTA including PBP, PIF and PN sub-regions using electrophysiology and genomic analysis [4]–[8], [26]. These studies suggested that PIF and especially the PN regions of VTA were more involved with the nicotine-exposure-related DA release. In order to image and quantify the neural activity in the VTA area with better resolution, we designed and implement this novel miniature implantable microimaging device.

Initially, we focused on the interaction of the fluorescence difference (ΔF) with the amount of nicotine intake. We noted the fluorescence intensity increased following the nicotine administration at increasing concentrations (0.07 - 0.63 mg/kg). We measured and compared the changes in the fluorescence intensity over the first 10 minutes. In Fig. 5(A), we observed the most noticeable changes in the GCaMP reaction was caused by the highest nicotine intake (0.63 mg/kg) in 10 minutes, which was consistent with a previous study [16]. We estimated the average fluorescence ratio ($\Delta F/F_0$ (%)) over 1 minute time window in a ROI to represent parts of whole images areas shown in Fig 5(B). Each ROI consisted of 9 x 9 pixels and was selected due to the highest fluorescent intensity. Fig. 5(B) shows the fluorescence ratio (%), $\Delta F/F_0$, of the ROI in each condition. The fluorescence ratio slightly decreased in the control (saline) data because of photo bleaching (i.e. prior to nicotine exposure). However, there was an increase in the fluorescence ratio after the nicotine administration. These findings were consistent with another previous study which used 0.6 mg/kg nicotine to excite DA release [27]. Therefore, we decided to use the 0.63 mg/kg dose for future studies.

Moreover, we calculated fluorescence ratios for 50 minutes after 0.63 mg/kg of nicotine to confirm that higher fluorescence intensity can still be observed after 10 minutes [16]. We used our implantable microimaging device to specifically observe the PIF and PN regions because these sub-regions have been associated with a high DA-nicotine response. Fig. 6(A) shows the fluorescence images and fluorescence difference (ΔF) of the ROI using 0.63 mg/kg of nicotine from one representative rat. We estimated the average fluorescence ratio ($\Delta F/F_0$ (%)) over 5 minutes time window in three different ROIs to represent the above (ROI1), middle (ROI2) and lower (ROI3) parts of whole images areas shown in Fig 6(B). Each ROI consisted of 9 x 9 pixels and was selected due to the highest fluorescence intensity within each region (high, middle, low). The average fluorescence ratio following 0.63 mg/kg nicotine administration showed a significant increase in the fluorescence ratio during the first 6-10 minutes and a gradual decrease after 31-35 minutes,

which continued for 50 minutes for all these three regions ($p<0.0001$). Additionally, ROI3 consistently had higher average fluorescence ratio compared to ROI1 at all time points ($p<0.0001$), and ROI3 was significantly higher than ROI2 at all time points ($p<0.05$), with the exception of the earliest time bin (i.e. 0-5 minutes). The theoretical position of the implantable microdevice within the brain is illustrated in Fig. 6(C).

This data provides valuable evidence that GCaMP fluorescence imaging after the nicotine administration can be observed during the first few minutes following nicotine exposure by using our novel implantable microimaging device.

B. THE POSITION OF IMPLANTED DEVICE AND GCaMP PRESENCE IN THE VTA

In order to confirm the position of the device and the presence of GCaMP, we used AAV-injected rats and performed GCaMP fluorescence imaging experiments. AAV-GCaMP expressions were clearly observed in VTA by using our implantable microimaging device as illustrated in Fig. 5(A) and Fig. 6(A). Then, to prove that the fluorescence reaction was produced by the GCaMP expression in the VTA, we confirmed the position of the device and the presence of GCaMP. Fig. 7 shows the bright field image of a coronal brain slice from a rat brain that was extracted after the implantation experiment. Animals were sacrificed and the brains sliced as detailed in the methods section. Representative figures of the fluorescence of GCaMP within the VTA are provided in Fig. 8(A) at 10X magnification, and Fig. 8(B), 20X magnification. At 20X magnification, a small scar in the brain made by the microimaging device was more apparent, as well as the greater fluorescence reaction in the VTA. Altogether, these results suggest that the device was inserted at the targeted region of the brain, i.e. the VTA. Moreover, we showed that it was possible to observe GCaMP fluorescence reactions by using our novel implantable microimaging device. Thus, this data suggests our implantable imaging device can capture the fluorescence reaction in the VTA associated with neural activities caused by nicotine administration.

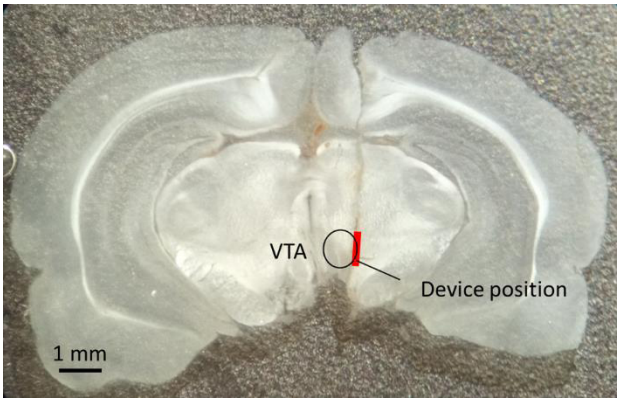

FIGURE 7. Bright field image of a rat coronal brain slice that was extracted after the implantation of our novel microimaging device. The VTA is circled and the location of our device is marked as a red rectangle. The scale bar represents 1 mm.

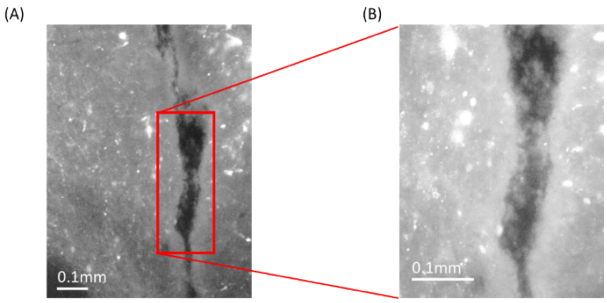

FIGURE 8. Fluorescence image of a brain slice. (A) Brain slices were obtained using a vibrotome to confirm the position of the implantable microimaging device and the GCaMP expression. The magnification was 10X. The scale bar represents 0.1 mm. (B) The magnified image of the brain sliced using 20X magnification. Please note that the small scar in the brain showed that the device was inserted at the VTA and the expression of GCaMP was observed in the brain tissues. The scale bar represents 0.1 mm.

IV. DISCUSSION

Nicotine has been widely reported to stimulate the neuronal firing rate of DA and increase DA release in the VTA, which is an important mechanism in drug reward and addiction [4]–[8], [26]. However, the underlying rewards mechanism has not been fully understood due to complex gene-regulatory networks, and their downstream molecular pathways and interactions, as well as the anatomy and physiology of the mesolimbic system involved with addiction.

In this study, we investigated the behavior of the DA neurons in response to nicotine exposure in different sub-regions of VTA, specifically the PBP, PIF and PN to understand the deep brain functional changes using a novel microimaging device. We introduced pAAV.CAG.GCaMP6s.WPRE. to wild type rats in order to image GCaMP fluorescence by using our implantable microimaging device and recorded the changes in the fluorescence associated with nicotine intake. We administered increasing concentrations of nicotine to the animals and recorded the GCaMP fluorescence over 50 minutes using our novel implantable microimaging devices. We observed a significant increase in fluorescence intensity during the first 10 minutes following exposure, and a decrease beginning after 30 minutes until the end of the measurement at 50 minutes following nicotine exposure. This data suggests maximal fluorescence within the VTA occurred between 6-10 minutes following nicotine exposure. Additionally, we observed that the fluorescent intensity observed in ROI3, corresponding to the lower area (PN) of the VTA, was higher compared to the other two areas corresponding to the PIF and PIN (Fig. 6(B)).

Using an implantable device, we determined that changes in the fluorescence reaction was related to nicotine intake and could be observed in VTA. According to these results, maximum $\Delta F/F_0$ was 19.7% when 0.63 mg/kg of nicotine was administered. However, this result was lower than what has been reported in the literature [16]. Wei *et al.*, showed

that at the high dose of nicotine the production of GCaMP increased approximately 55% [16]. The difference in these two studies could be due to the background intensity. Both fluorescence microscopy and the implantable microimaging device can measure changing of fluorescence intensity. However, background intensity of the implantable microimaging device is higher than that of fluorescence microscopy. In fluorescence microscopy, ΔF is calculated by considering only the fluorescence ratio intensities since the background value is close to 0 (Eq. 1). However, the background value (B) of the implantable microimaging device cannot be considered 0 because of the excitation light leakage. Then, $\Delta F/F_0$ for implantable microimaging device was calculated by Eq. 2(A) and (B). F' and F_0 indicated unmeasured fluorescence intensity by the implantable microimaging device. Therefore, it is possible that $\Delta F/F_0$ of the implantable microimaging device resulted with a decreased intensity rate in GCaMP compared to Wei *et al.*, results [16].

$$F = F^{'}+\mathrm{B}, F_0 = F_0^{'}+\mathrm{B} \qquad \text{(Eq. 2(A))}$$

$$\frac{\Delta F}{F_0} = \frac{\left(F'+B\right)-\left(\quad F_0'+B\right)}{F_0'+B} = \frac{F'-F_0'}{F_0'+B} \qquad \text{(Eq. 2(B))}$$

In our study, both DA neurons and GABA neurons were also marked by GCaMP since we introduced pAAV.CAG.GCaMP6s.WPRE. to wild type rats. Previous studies have shown that nicotine acts predominantly on dopamine neurons compared with GABA neurons [26]. Therefore, although we can argue that the results of fluorescence imaging data included the response from GABA neurons, it has been reported that most of the responses came from dopamine neurons. We first performed GCaMP fluorescence imaging with pAAV.CAG.GCaMP6s.WPRE. using wild-type rats, for further studies we are planning to use Dopamine Transporter (DAT) Cre-Rat. This rat model expresses Cre-recombinase under the control of the endogenous dopamine transporter promoter enabling specific expression in dopaminergic neurons. We will focus on only dopamine neural activity by using combination of DAT-Cre rat and GCaMP in our future studies. Using this transgenic animal model will also allow uniform distribution of GCaMP throughout the tissue during future studies. Additionally, it will help us to understand the neural activities in the three sub-regions in the VTA.

The actual spatial resolution of the device is approximately 22.3 micrometers, which is larger than the size of a soma. Though it may not be sufficient to observe the activities of individual neurons in the VTA, it can provide very useful information about the synchronizing neural activities from multiple neurons in the region of interest in response to substance intake including nicotine.

V. SUMMARY

In this study, we demonstrated that GCaMP fluorescence can be used to observe DA neuron activity associated with nicotine intake in VTA sub-regions using a novel implantable microimaging device. We used a combination of AAV and a dedicated microimaging device to observe neural activities within the vertical plane of VTA. GCaMP fluorescence reactions related to nicotine intake were observed by using a novel implantable microimaging device. The methods introduced in this study will be used to investigate the neural activities of the VTA during early maturation in response to nicotine and alcohol in future studies.

ACKNOWLEDGMENT

The authors would like to thank to the VLSI Design and Education Center (VDEC), The University of Tokyo, Cadence Corporation, and Mentor Graphics Corporation for their kind support. The authors are also grateful to Drs. Naze G. Avci and Charlotte Mae K. Waits for their assistance editing this manuscript.

REFERENCES

[1] H. A. Navarro, F. J. Seidler, W. L. Whitmore, and T. A. Slotkin, "Prenatal exposure to nicotine via maternal infusions: Effects on development of catecholamine systems," *J. Pharmacol. Exp. Therapeutics*, vol. 244, no. 3, pp. 940–944, 1988.

[2] S. A. Richardson and Y. Tizabi, "Hyperactivity in the offspring of nicotine-treated rats: Role of the mesolimbic and nigrostriatal dopaminergic pathways," *Pharmacol. Biochem. Behav.*, vol. 47, no. 2, pp. 331–337, Feb. 1994.

[3] K. Muneoka, T. Nakatsu, J.-I. Fuji, T. Ogawa, and M. Takigawa, "Prenatal administration of nicotine results in dopaminergic alterations in the neocortex," *Neurotoxicol. Teratol.*, vol. 21, no. 5, pp. 603–609, Sep. 1999.

[4] D. Zhang, M. Gao, D. Xu, W.-X. Shi, B. S. Gutkin, S. C. Steffensen, R. J. Lukas, and J. Wu, "Impact of prefrontal cortex in nicotine-induced excitation of ventral tegmental area dopamine neurons in anesthetized rats," *J. Neurosci.*, vol. 32, no. 36, pp. 12366–12375, Sep. 2012.

[5] H. Chen, S. L. Parker, S. G. Matta, and B. M. Sharp, "Gestational nicotine exposure reduces nicotinic cholinergic receptor (nAChR) expression in dopaminergic brain regions of adolescent rats," *Eur. J. Neurosci.*, vol. 22, no. 2, pp. 380–388, 2005.

[6] A. B. Gold, A. B. Keller, and D. C. Perry, "Prenatal exposure of rats to nicotine causes persistent alterations of nicotinic cholinergic receptors," *Brain Res.*, vol. 1250, pp. 88–100, Jan. 2009.

[7] A. Fallis, "Two projection systems from the ventral midbrain to the nucleus accumbens-olfactory tubercle complex," *J. Chem. Inf. Model.*, vol. 53, no. 9, pp. 1689–1699, 2013.

[8] D. Zhang, A. Dragomir, Y. M. Akay, and M. Akay, "Nicotine exposure increases the complexity of dopamine neurons in the parainterfascicular nucleus (PIF) sub-region of VTA," *J. NeuroEng. Rehabil.*, vol. 11, no. 1, pp. 1–6, 2014.

[9] K. Murari, R. Etienne-Cummings, G. Cauwenberghs, and N. Thakor, "An integrated imaging microscope for untethered cortical imaging in freely-moving animals," in *Proc. Annu. Int. Conf. IEEE Eng. Med. Biol.*, vol. 10, Aug. 2010, pp. 5795–5798.

[10] J. H. Park, J. Platisa, J. V. Verhagen, S. H. Gautam, A. Osman, D. Kim, V. A. Pieribone, and E. Culurciello, "Head-mountable high speed camera for optical neural recording," *J. Neurosci. Methods*, vol. 201, no. 2, pp. 290–295, Oct. 2011.

[11] K. K. Ghosh, L. D. Burns, E. D. Cocker, A. Nimmerjahn, Y. Ziv, A. E. Gamal, and M. J. Schnitzer, "Miniaturized integration of a fluorescence microscope," *Nature Methods*, vol. 8, no. 10, pp. 871–878, Oct. 2011.

[12] J. H. Jennings, R. L. Ung, S. L. Resendez, A. M. Stamatakis, J. G. Taylor, J. Huang, K. Veleta, P. A. Kantak, M. Aita, K. Shilling-Scrivo, C. Ramakrishnan, K. Deisseroth, S. Otte, and G. D. Stuber, "Visualizing hypothalamic network dynamics for appetitive and consummatory behaviors," *Cell*, vol. 160, no. 3, pp. 516–527, Jan. 2015.

[13] W. Zong, R. Wu, M. Li, Y. Hu, Y. Li, J. Li, H. Rong, H. Wu, Y. Xu, Y. Lu, H. Jia, M. Fan, Z. Zhou, Y. Zhang, A. Wang, L. Chen, and H. Cheng, "Fast high-resolution miniature two-photon microscopy for brain imaging in freely behaving mice," *Nature Methods*, vol. 14, no. 7, pp. 713–719, Jul. 2017.

[14] Y.-J. Luo, Y.-D. Li, L. Wang, S.-R. Yang, X.-S. Yuan, J. Wang, Y. Cherasse, M. Lazarus, J.-F. Chen, W.-M. Qu, and Z.-L. Huang, "Nucleus accumbens controls wakefulness by a subpopulation of neurons expressing dopamine D1 receptors," *Nature Commun.*, vol. 9, no. 1, Dec. 2018, Art. no. 1576.
[15] I. Ferezou, S. Bolea, and C. C. H. Petersen, "Visualizing the cortical representation of whisker touch: Voltage-sensitive dye imaging in freely moving mice," *Neuron*, vol. 50, no. 4, pp. 617–629, May 2006.
[16] C. Wei, X. Han, D. Weng, Q. Feng, X. Qi, J. Li, and M. Luo, "Response dynamics of midbrain dopamine neurons and serotonin neurons to heroin, nicotine, cocaine, and MDMA," *Cell Discovery*, vol. 4, no. 1, Dec. 2018.
[17] S. L. Resendez, J. H. Jennings, R. L. Ung, V. M. K. Namboodiri, Z. C. Zhou, J. M. Otis, H. Nomura, J. A. McHenry, O. Kosyk, and G. D. Stuber, "Visualization of cortical, subcortical and deep brain neural circuit dynamics during naturalistic mammalian behavior with head-mounted microscopes and chronically implanted lenses," *Nature Protocols*, vol. 11, no. 3, pp. 566–597, Mar. 2016.
[18] L. Lu, P. Gutruf, L. Xia, D. L. Bhatti, X. Wang, A. Vazquez-Guardado, X. Ning, X. Shen, T. Sang, R. Ma, G. Pakeltis, G. Sobczak, H. Zhang, D.-O. Seo, M. Xue, L. Yin, D. Chanda, X. Sheng, M. R. Bruchas, and J. A. Rogers, "Wireless optoelectronic photometers for monitoring neuronal dynamics in the deep brain," *Proc. Nat. Acad. Sci. USA*, vol. 115, no. 7, pp. E1374–E1383, Feb. 2018.
[19] J. Ohta, Y. Ohta, H. Takehara, T. Noda, K. Sasagawa, T. Tokuda, M. Haruta, T. Kobayashi, Y. M. Akay, and M. Akay, "Implantable microimaging device for observing brain activities of rodents," *Proc. IEEE*, vol. 105, no. 1, pp. 158–166, Jan. 2017.
[20] H. Takehara, Y. Ohta, M. Motoyama, M. Haruta, M. Nagasaki, H. Takehara, T. Noda, K. Sasagawa, T. Tokuda, and J. Ohta, "Intravital fluorescence imaging of mouse brain using implantable semiconductor devices and epi-illumination of biological tissue," *Biomed. Opt. Express*, vol. 6, no. 5, p. 1553, May 2015.
[21] A. Tagawa, A. Higuchi, T. Sugiyama, K. Sasagawa, T. Tokuda, H. Tamura, Y. Hatanaka, Y. Ishikawa, S. Shiosaka, and J. Ohta, "Development of complementary metal oxide semiconductor imaging devices for detecting green fluorescent protein in the deep brain of a freely moving mouse," *Jpn. J. Appl. Phys.*, vol. 48, no. 4, Apr. 2009, Art. no. 04C195.
[22] Y. Sunaga, H. Yamaura, M. Haruta, T. Yamaguchi, M. Motoyama, Y. Ohta, H. Takehara, T. Noda, K. Sasagawa, T. Tokuda, Y. Yoshimura, and J. Ohta, "Implantable imaging device for brain functional imaging system using flavoprotein fluorescence," *Jpn. J. Appl. Phys.*, vol. 55, no. 3S2, Mar. 2016, Art. no. 03DF02.
[23] M. Haruta, Y. Kurauchi, M. Ohsawa, C. Inami, R. Tanaka, K. Sugie, A. Kimura, Y. Ohta, T. Noda, K. Sasagawa, T. Tokuda, H. Katsuki, and J. Ohta, "Chronic brain blood-flow imaging device for a behavioral experiment using mice," *Biomed. Opt. Express*, vol. 10, no. 4, p. 1557, Apr. 2019.
[24] M. Haruta, Y. Sunaga, T. Yamaguchi, H. Takehara, T. Noda, K. Sasagawa, T. Tokuda, and J. Ohta, "Intrinsic signal imaging of brain function using a small implantable CMOS imaging device," *Jpn. J. Appl. Phys.*, vol. 54, no. 4S, Apr. 2015, Art. no. 04DL10.
[25] M.-C. Giroux, P. Hélie, P. Burns, and P. Vachon, "Anesthetic and pathological changes following high doses of ketamine and xylazine in Sprague Dawley rats," *Exp. Animals*, vol. 64, no. 3, pp. 253–260, 2015.
[26] R. F. Keller, T. Kazemi, A. Dragomir, Y. M. Akay, and M. Akay, "Comparison between dopaminergic and non-dopaminergic neurons in the VTA following chronic nicotine exposure during pregnancy," *Sci. Rep.*, vol. 9, no. 1, pp. 1–13, Dec. 2019.
[27] M. Subramaniyan and J. A. Dani, "Dopaminergic and cholinergic learning mechanisms in nicotine addiction," *Ann. New York Acad. Sci.*, vol. 1349, no. 1, pp. 46–63, Sep. 2015.

YOSHINORI SUNAGA received the B.E. degree from Chiba University, Japan, in 2012, and the M.E. and Ph.D. degrees from the Graduate School of Materials Science, Nara Institute of Science and Technology (NAIST), Japan, in 2014 and 2017, respectively. In 2017, he joined NAIST as a Postdoctoral Fellow, and starts collaboration research between NAIST and the University of Houston. In 2019, he joined the University of Houston as a Postdoctoral Fellow. He is interested in the development of novel devices for observing and accessing brain activity of animals to reveal new brain mechanism.

YASUMI OHTA received the Ph.D. degree in biophysics science from Kyoto University, Kyoto, Japan, in 2011. In 2011, she joined the Nara Institute of Science and Technology, Nara, Japan, as a Postdoctoral Fellow. Her research interests involve implantable bioimaging CMOS sensors and neuroscience

YASEMIN M. AKAY (Member, IEEE) received the B.S. degree in pharmaceutical sciences from Hacettepe University, Ankara, Turkey, in 1980, and the M.S. and Ph.D. degrees in biomedical engineering from Rutgers University, Piscataway, NJ, USA, in 1991 and 1998, respectively. She is currently an Instructional and Research Assistant Professor with the Department of Biomedical Engineering, Cullen College of Engineering, University of Houston, Houston, TX, USA. She was a Postdoctoral Fellow at the Physiology and Pharmacology Departments, Dartmouth Medical School, and at the Department of Physiology and Biophysics, School of Medicine, Boston University. Her current research interests include molecular neuroengineering, neural growth, and neurodegeneration. She was an Assistant Editor of the IEEE book series, from September 2001 to May 2004, and has been a Managing Editor of the *Wiley Encyclopedia of Biomedical Engineering*, since May 2004.

JUN OHTA (Senior Member, IEEE) received the B.E., M.E., and Dr.Eng. degrees in applied physics from The University of Tokyo, Japan, in 1981, 1983, and 1992, respectively. In 1983, he joined Mitsubishi Electric Corporation, Hyogo, Japan. From 1992 to 1993, he was a Visiting Scientist with the Optoelectronics Computing Systems Center, University of Colorado at Boulder. In 1998, he joined the Graduate School of Materials Science, Nara Institute of Science and Technology (NAIST), Nara, Japan, as an Associate Professor. He was appointed as a Professor, in 2004. His current research interests are smart CMOS image sensors for biomedical applications and retinal prosthetic devices. He is a Fellow of the Japan Society of Applied Physics and the Institute of Image, Information, and Television Engineers. He serves as an Associate Editor of the IEEE TRANSACTIONS ON BIOMEDICAL CIRCUITS AND SYSTEMS, and an Editorial Board of *Journal of Engineering*, IET.

METIN AKAY (Fellow, IEEE) received the B.S. and M.S. degrees in electrical engineering from Bogazici University, Istanbul, Turkey, in 1981 and 1984, respectively, and the Ph.D. degree from Rutgers University, Piscataway, NJ, USA, in 1990. He is the Founding Chair of the Department of Biomedical Engineering, University of Houston. His current research focus on the investigation of nicotine and alcohol addiction at the molecular, cellular and system levels during maturation, and the development of brain chip for precision medicine. He is the President-Elect of the IEEE EMBS. He was the Founding Chair of the Annual International Summer School on BIO-X, sponsored by the National Science Foundation (NSF) and technically co-sponsored by the IEEE EMBS, of the Satellite Conference on Emerging Technologies in Biomedical Engineering. He is also the Founding Chair of the International IEEE Conference on Neural Engineering, in 2003.